Angewandte Chemie
Eine Zeitschrift der Gesellschaft Deutscher Chemiker

Supporting Information

Highly Dispersed ZnO Sites in a ZnO/ZrO_2 Catalyst Promote Carbon Dioxide-to-Methanol Conversion

X. Zhang, X. Yu, R. G. Mendes, P. Matvija, A. E. M. Melcherts, C. Sun, X. Ye, B. M. Weckhuysen, M. Monai**

Supporting Information to

Highly Dispersed ZnO Sites in a Zn/ZrO_2 Catalyst Promote the Carbon Dioxide-to-Methanol Reaction

Xibo Zhang[a,b], Xiang Yu[a], Rafael G. Mendes[c], Peter Matvija[d], Angela E.M. Melcherts[a], Chunning Sun[a], Xinwei Ye[a], Bert M. Weckhuysen[a],* and Matteo Monai[a],*

[a] Inorganic Chemistry and Catalysis Group, Institute for Sustainable and Circular Chemistry, Utrecht University, Universiteitsweg 99, Utrecht 3584 CG Utrecht , The Netherlands

[b] State Key Laboratory of Physical Chemistry of Solid Surfaces & Department of Chemistry, College of Chemistry and Chemical Engineering, Xiamen University, Xiamen 361005, P. R. China.

[c] Soft Condensed Matter Group, Debye Institute for Nanomaterials Science, Utrecht University, Heidelberglaan 8, 3584 CS Utrecht, The Netherlands

[d] Charles University, Faculty of Mathematics and Physics, Department of Surface and Plasma Science, V Holešovičkách 2, Prague, Czech Republic

*email: b.m.weckhuysen@uu.nl, m.monai@uu.nl

1. Catalyst Material Synthesis

1.1 Chemicals, gases and materials

Zirconium oxychloride ($ZrOCl_2 \cdot 8H_2O \geq 99.5\%$), zinc nitrate hexahydrate ($Zn(NO_3)_2 \cdot 6H_2O \geq 99.0\%$) and ammonia solution (32%) were purchased from Sigma-Aldrich. Commercial monoclinic zirconia (99%) was purchased from Alfa Aesar. All chemicals were used without further purification. Demineralized water was purified with a Milli-Q system (18.2 MΩ) before use. The purity of gas used in experiments are N_2 (Linde, purity 99.998%), H_2 (Linde, purity 99.999%), CO_2 (Linde, purity 99.9993%) and He (Linde, purity 99.999%) and Ar (Linde, purity 99.998%).

1.2 Material synthesis

1.2.1 Synthesis of tetragonal ZrO_2 (ZrO_2-t)

24.17 g of $ZrOCl_2 \bullet 8H_2O$ was dissolved in 150 mL of aqueous solution, poured into 50 mL of ammonia solution under stirring and continued to stir for 3 h. Then, the solution was refluxed at 100 °C for 48 h, and samples were collected by centrifugation after cooling down to room temperature. Finally, the collected samples were calcined in a muffle furnace at 600 °C for 5 h to ensure a full conversion of the precursor compound and to form a phase-pure ZrO_2-t material.

1.2.2 Synthesis of ZnO/ZrO_2

0.59 g of $Zn(NO_3)_2 \cdot 6H_2O$ was dissolved in 2 mL of water, then added dropwise to 2 g of ZrO_2-t, stirred manually, and left to stand for 3 h, then dried in an oven at 60 °C. Finally, the sample was calcined in a tube furnace at 400 °C

for 2 h under the mixed gas of N_2 and O_2, and the obtained sample was named ZnO/ZrO_2-t. For ZrO_2 loaded in the monoclinic phase, ZrO_2-m was calcined at 550 °C for 2 h in a muffle furnace to eliminate surface adsorbed impurities. The method of loading ZnO is the same as the above synthesis method, and the final sample is named ZnO/ZrO_2-m.

2. Catalyst Material Testing

Catalytic tests for the CO_2 hydrogenation reaction were performed at 20 bar using a laboratory-built high-pressure apparatus. 1 g of catalyst sample, with a sieved particle size of 75–212 μm, was placed between two plugs of quartz wool in a steel fixed bed reactor. A back pressure regulator was used to control the pressure. Product analysis was performed using an online Thermo Fischer Trace 1300 gas chromatograph (GC). The effluent streams were analyzed by gas chromatography every 27 min. The performance of the catalyst material is based on the average of three points taken after reaction temperature stabilization. The pressure was increased to 20 bar at room temperature, at a rate of 1 bar min^{-1} in a CO_2/H_2/Ar mixed atmosphere (7.2:21.6:1.2 mL min^{-1}, GHSV: 1800 h^{-1}). Afterwards, the system was heated up to the reaction temperature at a rate of 5 °C min^{-1}. No reduction pretreatments were performed on the catalysts. The selectivity and space time yield (STY) were defined in the following equation:

$$Con._{(CO_2,\%)} = \left(1 - \frac{A_{t(CO_2)} / A_{t(Ar)}}{A_{0(CO_2)} / A_{0(Ar)}}\right) \times 100\%$$

$$Sel._{(CH_3OH,\%)} = \left(\frac{A_{t(CH_3OH)} \times f_{(CH_3OH)}}{A_{t(CH_3OH)} \times f_{(CH_3OH)} + A_{t(CO)} \times f_{(CO)}}\right) \times 100\%$$

$$STY_{(CH_3OH,mmol/g/h)} = \frac{A_{t(CH_3OH)} \times f_{(CH_3OH)} \times V_{(gas,\,ml/min)} \times 60}{m_{(cat,\,g)} \times 22.4}$$

where $A_{t(Ar)}$, $A_{t(CO_2)}$, $A_{t(CO)}$ and $A_{t(CH_3OH)}$ are the peak areas of Ar, CO_2, CO and

CH_3OH on the GC data at t time during the reaction, respectively. $A_{t(Ar)}$ and $A_{t(CO_2)}$ are the peak areas of Ar and CO_2 on GC data before reaction, respectively. f_{CO} and f_{CH_3OH} are the calibration factors of CO and CH_3OH. $V_{(gas)}$ is the volumetric flow of feed gas (mL min^{-1}) and $m_{(cat,g)}$ is the amount of catalyst.

3. Catalyst Material Characterization and Modelling

3.1 Catalyst characterization.

Energy dispersive X-ray (EDX) spectroscopy were obtained using a Phenom ProX microscope with an acceleration voltage of 10 kV equipped with a EDX detector. Transmission electron microscopy (TEM) images were collected on a Tecnai20F transmission electron microscope, operated at a voltage of 200 kV. The high-resolution High-Angle Annular Dark-Field Scanning Transmission Electron Microscopy (HAADF-STEM) imaging, EDX and elemental mapping were performed with a monochromated Thermo Fisher Scientific Spectra300 TEM instrument operating with an acceleration voltage of 300 kV and equipped with a SuperX EDX detector. X-ray diffraction (XRD) patterns were recorded with Bruker D8 Phaser diffractometer equipped with a Cu K_α source (λ=1.54056 Å). Diffraction patterns of catalysts were recorded between 10 and 90° with an increment of 0.05° and 1 s/step. Raman spectra was measured by a Renishaw inVia Raman microscope with a 785 nm excitation laser. The surface area of the samples were measured with a Micromeritics TriStar 3000. Before nitrogen physisorption, the samples were dried under vacuum at 300 °C overnight. The surface area was calculated with the Brunauer-Emmett-Teller (BET) method.

3.2. Operando diffuse reflectance infrared Fourier transform spectroscopy

Operando diffuse reflectance infrared Fourier transform spectroscopy (DRIFTS) was used to study the reaction intermediates and reaction products in the catalytic CO_2 hydrogenation to methanol reaction. A Bruker Tensor 37 FT-infrared (IR) spectrometer with diffuse reflectance (DR) in situ cell with mercury cadmium telluride (MCT) detector was used to record a spectrum every 1 min. On-line product analysis was performed using a Global Analyzer Solutions (G.A.S.) Compact 4.0 GC instrument custom-built by Interscience. In a typical experiment, 20 mg of sample was loaded in a dome Harrick cell equipped with high-pressure windows. The pressure was increased to 10 bar at room temperature, at a rate of 1 bar min^{-1} in a CO_2/H_2/Ar mixed atmosphere (5:15:1 mL min^{-1}). Afterwards, the system was heated up to the reaction temperature at a rate of 5 °C min^{-1}. No reduction pretreatments were performed on the catalyst materials before characterization. For the calculation of the IR areas in Figure 4d and Figure S15, first, the spectra were baseline subtracted using a polynomial curve, to adjust the baseline intensity of the absorption spectrum to 0, then, the bands were integrated using the following spectral ranges: 2794–2913 cm^{-1} for the 2887 cm^{-1} band, 2142–2219 cm^{-1} for the 2174 cm^{-1} band, and 1405–1502 cm^{-1} for the 1446 cm^{-1} band.

3.3. Operando UV-Vis diffuse reflectance spectroscopy

For operando UV-Vis diffuse reflectance spectroscopy (DRS) experiments,

100 mg the catalyst was sieved to a particle size of 75–212 μm, placed in a quartz tube, and quartz wool was placed on top of the sample. an AvaLight-DH-S-BAL light source was used as light source for the UV-Vis measurements, and a high-temperature UV–Vis fiber optics probe was used to carry the light to the sample from a window on the reactor side, and the product is detected by on-line GC making use of a Global Analyzer Solutions (G.A.S.) Compact GC 4.0 instrument. The DRS mode of the Lambda 950S spectrometer was used to detect the structural change of the catalyst material during CO_2 hydrogenation under normal pressure. A UV-Vis spectrum was detected every 30 s.

3.4. Temperature programmed desorption (TPD) of NH_3

Ammonia Temperature-Programmed Desorption (NH_3 TPD) was conducted using a Micromeritics AutoChemII 2920. In each experiment, around 80 mg of the sample was used. The sample was initially pretreated in He (25 mL min^{-1}) for 1 h at 400 °C, followed by cooling to 100 °C. It was then saturated with ammonia until equilibrium was reached. Before desorption, the samples were flushed with He for 30 minutes. Ammonia desorption was subsequently carried out from 100 °C to 700 °C at a heating rate of 10 °C min^{-1}. The desorption amount of the NH_3 was determined simultaneously by the thermal conductivity detector.

3.5. Temperature programmed desorption of CO_2

A similar procedure to that used for NH_3 TPD was applied for carbon dioxide Temperature-Programmed Desorption (TPD) (CO_2 TPD). In each experiment, around 80 mg of the sample was used. The sample was initially pretreated in He (25 mL min^{-1}) for 1 h at 400 °C, followed by cooling to 50 °C. It was then saturated with CO_2 until equilibrium was reached. Before desorption, the samples were flushed with He for 30 minutes. CO_2 desorption was subsequently carried out from 50 °C to 700 °C at a heating rate of 10 °C min^{-1}. The amount of the CO_2 was determined simultaneously by the thermal conductivity detector.

3.6. Temperature programmed reduction (TPR) of H_2

Temperature-programmed reduction of hydrogen (H_2 TPR) experiments were performed on a Altamira instrument AMI-300. About 80 mg sample was loaded into a U-shape quartz reactor and heated to 400 °C under an Ar flow of 30 mL min^{-1} for 1 h to remove adsorbed species. After cooling to 50 °C, the flowing gas was then switched to a 5 vol.% H_2/Ar mixture, and the catalyst was heated to 700 °C at a ramping rate of 10 °C min^{-1}. The amount of the H_2 was determined simultaneously by the thermal conductivity detector.

3.7. Transmission electron microscopy

The bright field transmission electron microscopy (TEM) images, the aberration corrected high-angle annular dark field scanning transmission

electron microscopy (AC-HAADF-STEM) images, and the energy-dispersive X-ray spectroscopy (EDX) elemental mappings were acquired utilizing a Thermo Fisher Scientific Spectra 300 microscope operating at 300 kV. All measurements were conducted with a 0° tilt angle. The bright field TEM images were acquired with a total exposure time of 1 s using a Thermo Fisher Scientific Complementary Metal-Oxide-Semiconductor (CMOS) Ceta 16M camera. Conversely, the AC-HAADF-STEM images were captured with a dwell time of 20 µs per pixel, a spot size of 9, a camera length of 91 mm, and a convergence angle of 21.8 mrad. The HAADF-EDX elemental mappings were acquired using a segmented SuperX G2 detector with identical parameters mentioned above, except for reduced dwell time (2 µs/pixel) aimed at mitigating potential beam damage and contamination during the acquisition. Data analysis was performed using the Thermo Fisher Scientific software, VELOX (v 3.6.0).

3.8. Near-ambient pressure X-ray photoelectron spectroscopy

Near-ambient pressure X-ray photoelectron spectroscopy (NAP-XPS) measurements were performed on a custom-built Specs spectrometer using a DeviSim NAP reactor cell coupled with a differentially pumped hemispherical electron energy analyzer (Phoibos 150 NAP 2D-DLD) and an Al K_α X-ray source (µ-Focus 600). Samples were transferred to the NAP cell via ultra-high vacuum (UHV) chambers with the base pressure of 1×10^{-9} mbar. During measurements, the samples were situated at a distance of 0.3 mm from an electron-collecting

nozzle having an orifice diameter of 0.3 mm. The NAP cell was working in a dynamic mode with the completely open pumping outlet, while the required gas pressure was set using a proper inlet flow of gases. Samples were exposed to pure CO_2 (Linde, purity 99.9993%) and H_2 (Linde, purity 99.999%) gases. The temperature of the samples was monitored by a K-type thermocouple mounted directly on the sample holder. All XPS data were corrected for charging by shifting all XPS peaks to the energy of the C 1s peak of C-C at 284.6 eV, because no adventitious carbon (usually used as reference) was detected after heating under hydrogen. All fitting parameters, except for amplitude, were fixed for all presented spectra.

3.9. Density functional theory calculations

Ab initio density functional theory (DFT) calculations were performed using the Vienna Ab-initio Simulation Package (VASP) with the projector-augmented wave (PAW) method.[1] The Perdew-Becke Ernzerhof (PBE) exchange-correlation functional was used.[2] The (111) surface of ZrO_2-m and (101) surface of ZrO_2-t were optimized and used as supports in the models, because of their low surface energy.[3] 25 Å of vacuum in the z direction was used to separate the slab, to prevent interaction among adsorbed intermediates. The (001) surface of ZnO was used for the study potential energy of H_2 dissociation on ZnO.[4]

The favorable adsorption sites of isolated Zn atom centers were tested on both ZrO_2 slabs. The slabs were composed of 8 Zr layers, and the bottom two

Zr layers were fixed during geometric optimization. The kinetic energy cutoff for the plane wave basis set for all calculations was 600 eV. The Monkhorst-Pack mesh k-points of (3 × 3 × 1) for both Zn_1 and Zn_2 slabs were used to sample the surface Brilliouin zone. Conjugate gradient method was used for geometric optimization, the Hellman–Feynman forces on each ion were converged to 0.03 eV•$Å^{-1}$ and electronic convergence was set at 10^{-6} eV. The Hessian matrix was constructed using a finite displacement approach with a step size of 0.02 Å for displacement of individual atoms along each Cartesian coordinate. These frequencies were used to determine the zero-point energy (ZPE) correction to the energy of the geometries of the initial, transition, and final states.

4. Supplementary Figures and Table

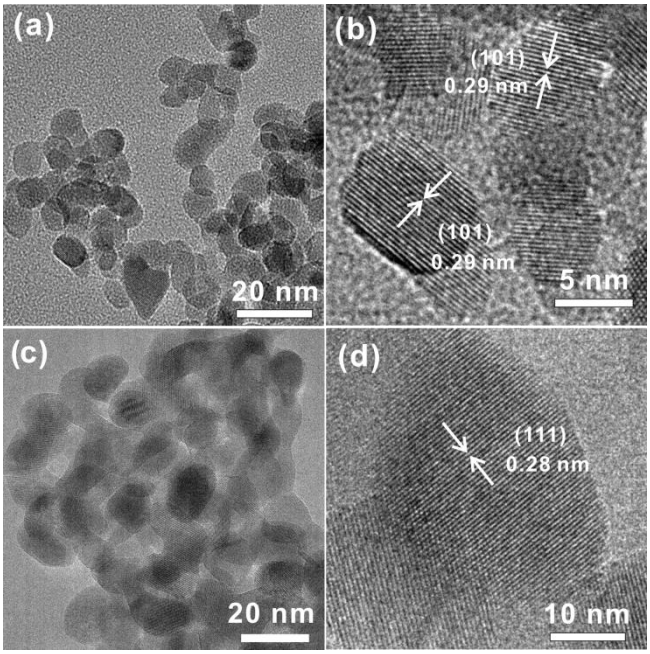

Figure S1. (a-b) TEM images of tetragonal ZrO_2 (ZrO_2-t), where the observed lattice fringes of 0.29 nm correspond to the (101) plane; (c-d) TEM images of monoclinic ZrO_2 (ZrO_2-m), where the lattice fringes of 0.28 nm correspond to the (111) plane.

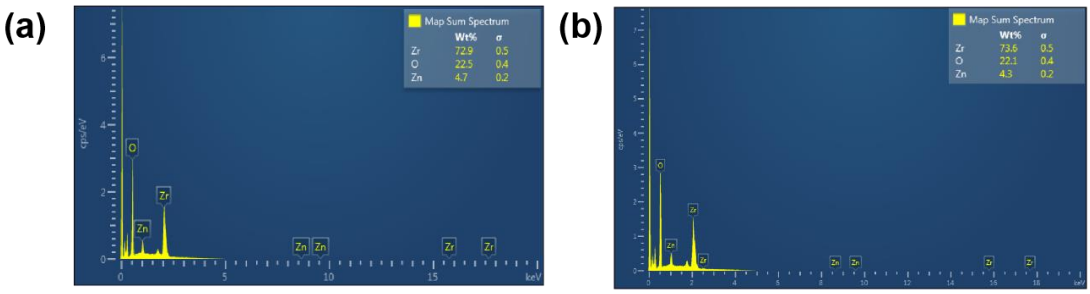

Figure S2. EDX spectroscopy results of (a) ZnO/ZrO_2-t and (b) ZnO/ZrO_2-m.

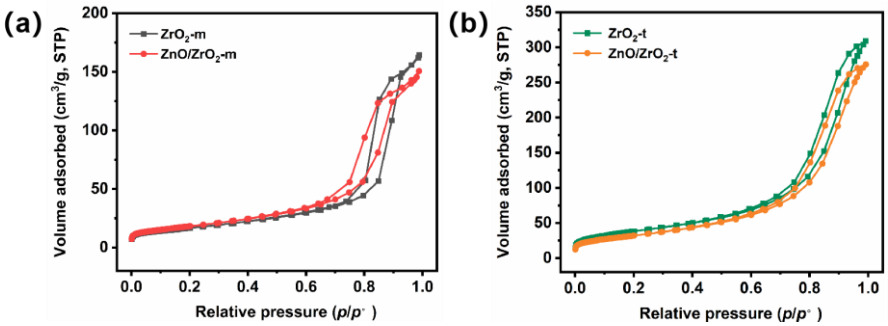

Figure S3. N_2 adsorption-desorption isotherms of (a) ZrO_2-m, ZnO/ZrO_2-m and (b)ZrO_2-t and ZnO/ZrO_2-t.

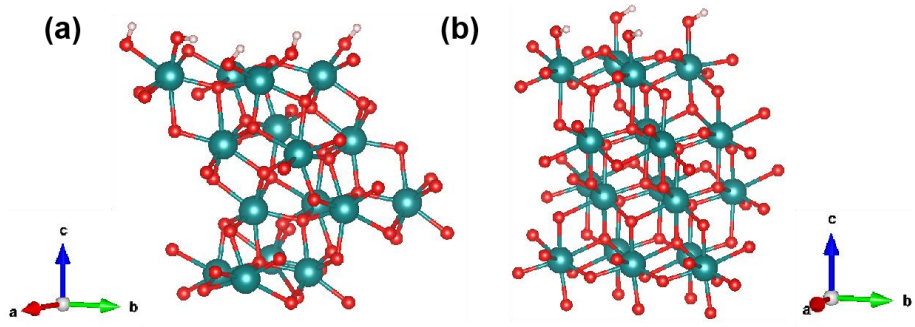

Figure S4. Optimized crystal structure of (a) ZrO_2-m (111) and (b) ZrO_2-t (101). Green balls, red balls and white balls represent Zr, O and H atoms, respectively.

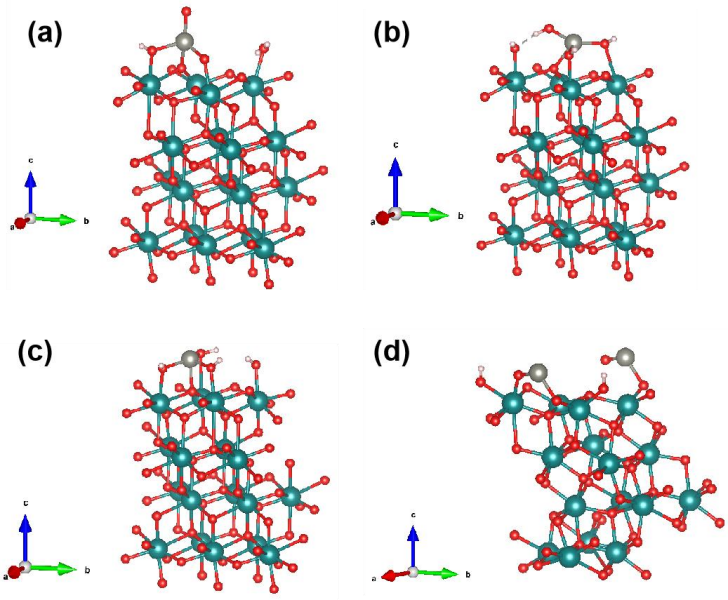

Figure S5. Optimized crystal structure of Zn adsorbed on (a-c) ZrO_2-t (101) and (d) ZrO_2-m (111). Grey balls, green balls, red balls and white balls represent Zn, Zr, O and H atoms, respectively.

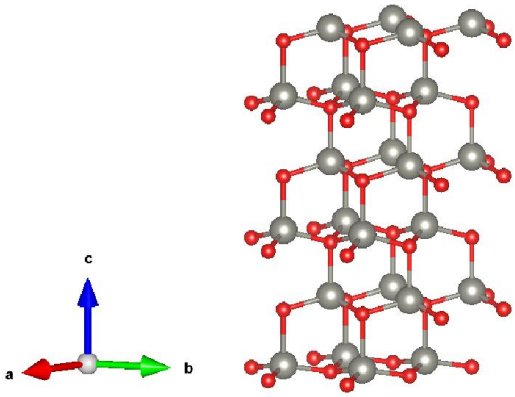

Figure S6. Optimized crystal structure of ZnO (001).

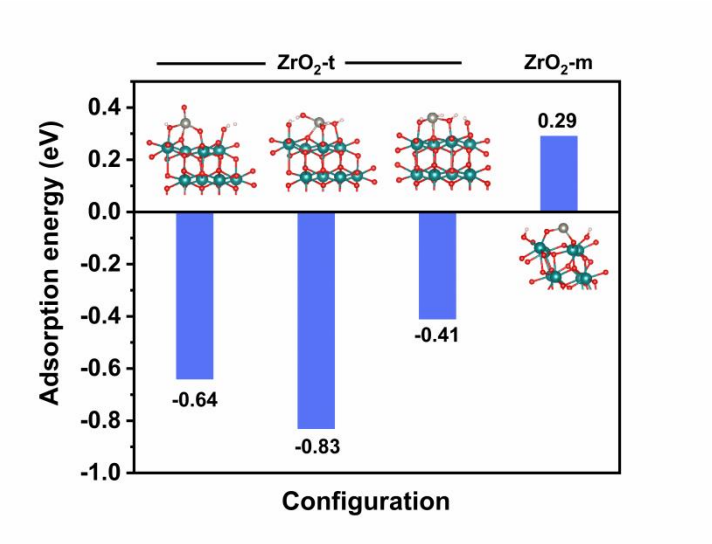

Figure S7. Adsorption energy of Zn on the tetragonal ZrO_2 (101) and monoclinic ZrO_2 (111) surfaces. Three models for the Zn atom on tetragonal ZrO_2 (101) include Zn replacing the hydrogen atom in the hydroxyl group and two arrangements where Zn directly coordinates with surface oxygen atoms.

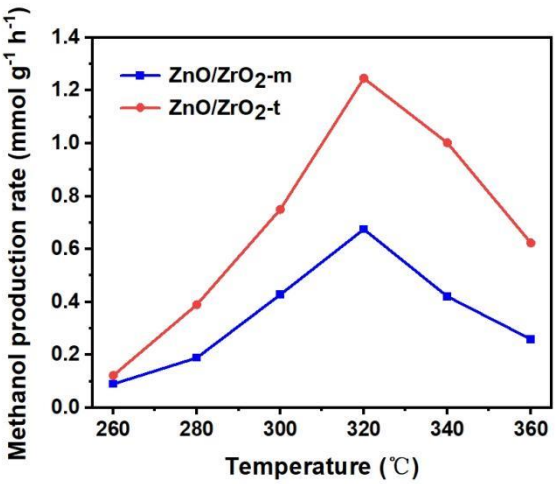

Figure S8. Production rate of CH_3OH at different reaction temperatures over ZnO/ZrO_2-t and ZnO/ZrO_2-m. (Reaction conditions: 1 g catalyst, reaction pressure = 20 bar, gas composition: CO_2:H_2=1/3, and GHSV: 1800 h^{-1})

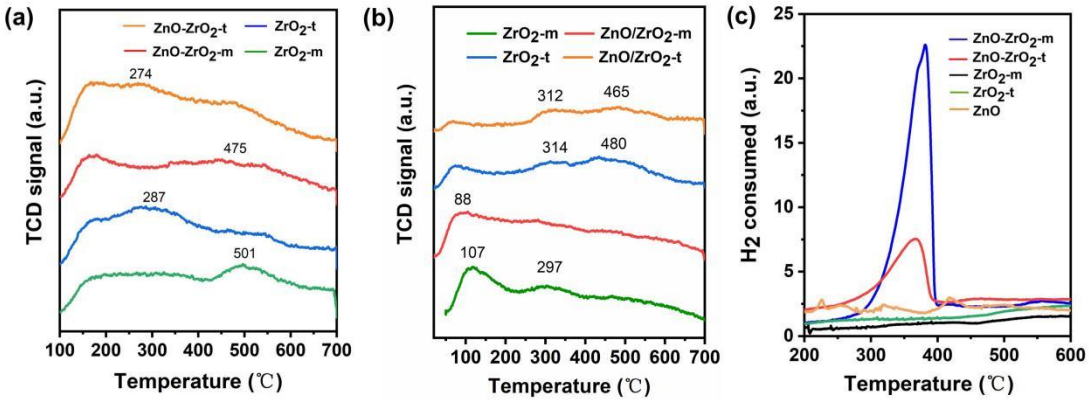

Figure S9. (a) TPD of NH_3, (b) TPD of CO_2 and (c) TPR of H_2 for the catalyst materials under study.

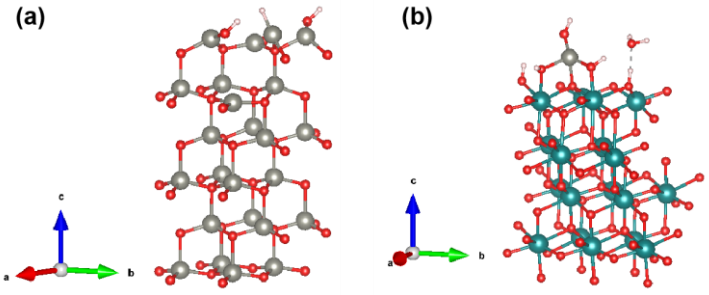

Figure S10. Optimized crystal structure of H_2 dissociated on (a) ZnO (001), (b) ZnO-ZrO site in ZnO/ZrO_2-t (101). Grey balls, green balls, red balls and white balls represent Zn, Zr,

O and H atoms, respectively.

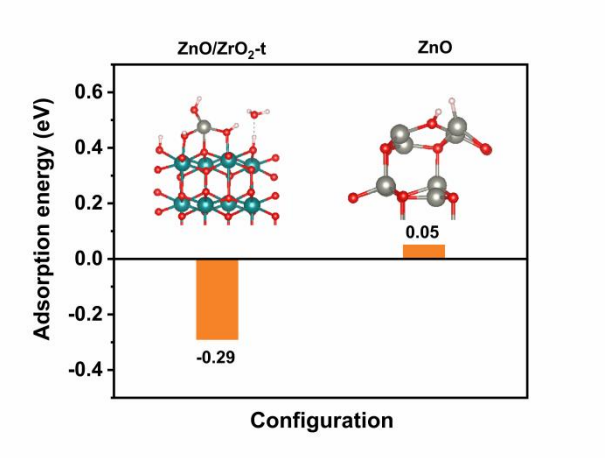

Figure S11. Adsorption energy of H_2 at a ZnO-ZrO site in the ZnO/ZrO_2-t (101) and on a ZnO (001) slab (see for more details section 3.9).

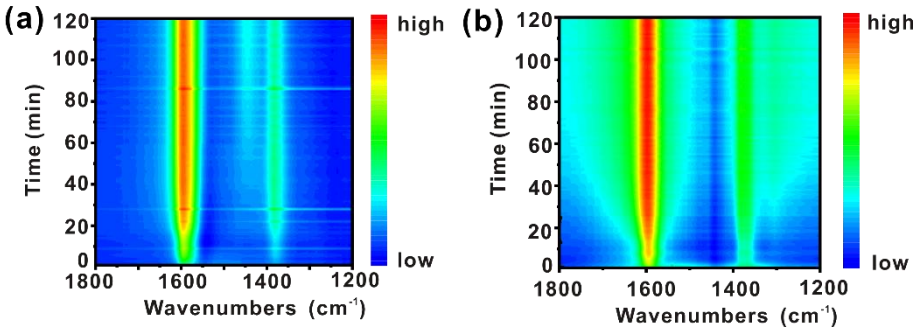

Figure S12. The respective contour plots for the spectral region of 1800–1200 cm^{-1} of the operando DRIFTS data of the ZnO/ZrO_2-t and ZnO/ZrO_2-m materials are shown in (a) and (b) for clarity.

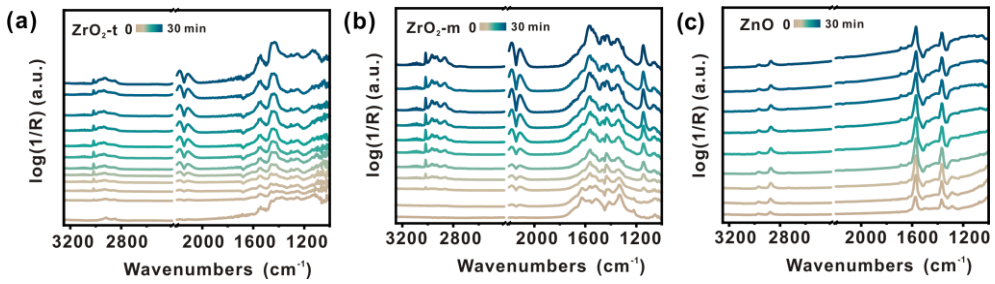

Figure S13. Operando DRIFTS spectra as a function of time during catalytic CO_2 hydrogenation over (a) ZrO_2-t, (b) ZrO_2-m and (c) ZnO catalyst materials (reaction conditions: CO_2/H_2=1/3, reaction temperature = 320 °C, reaction pressure = 10 bar, 1

spectrum min^{-1}).

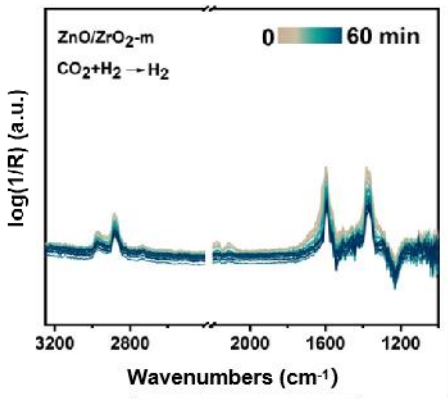

Figure S14. Operando DRIFTS data of the ZnO/ZrO_2-m material, when switching from CO_2+H_2 to H_2 at 320 °C and 10 bar.

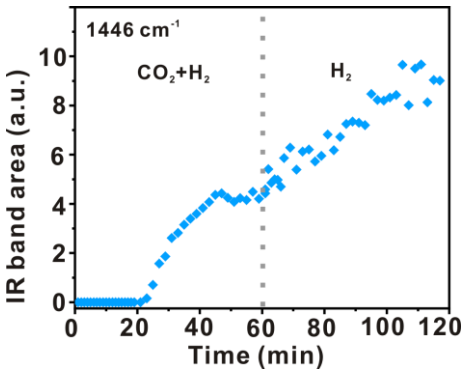

Figure S15. Area of the CO_3^{2-} infrared (IR) band (located at ~ 1446 cm^{-1}) over time.

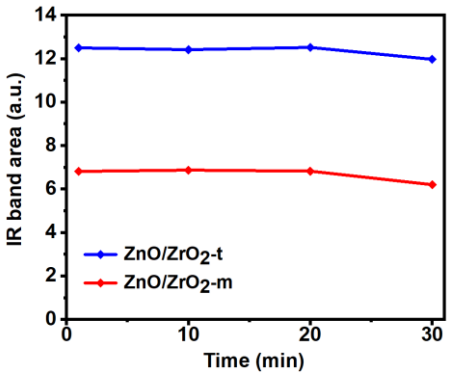

Figure S16. Area of the HCOO* IR band when switching from CO_2+H_2 to Ar at 320 °C (blue line: ZnO/ZrO_2-t, orange line: ZnO/ZrO_2-m).

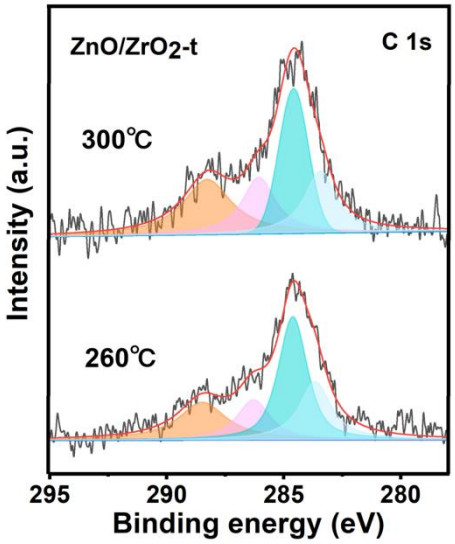

Figure S17. Deconvoluted in situ NAP-XPS data measured in the C 1s region of the ZnO/ZrO_2-t material at 300 °C and 260 °C in 0.25 mbar CO_2 + 0.75 mbar H_2.

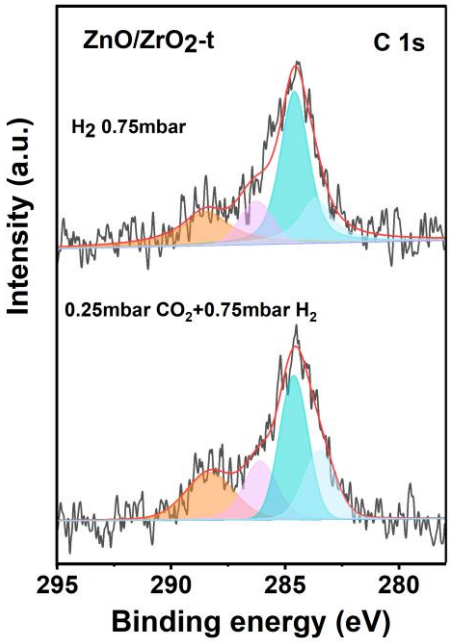

Figure S18. Deconvoluted in situ NAP-XPS data measured in the C 1s region of the ZnO/ZrO_2-t material when switching from CO_2 and H_2 to H_2 at 320 °C.

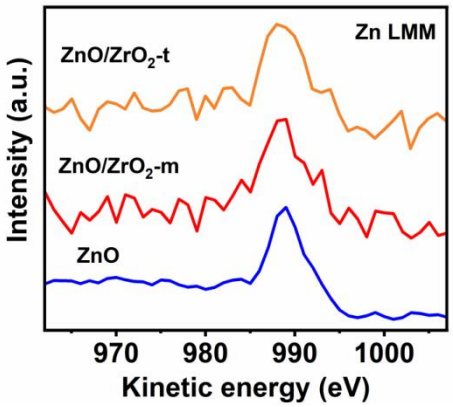

Figure S19. In situ NAP-XPS data measured in the Zn LMM region of the ZnO/ZrO_2-t, ZnO/ZrO_2-m and ZnO, measured at 320 °C in 0.25 mbar CO_2 + 0.75 mbar H_2.

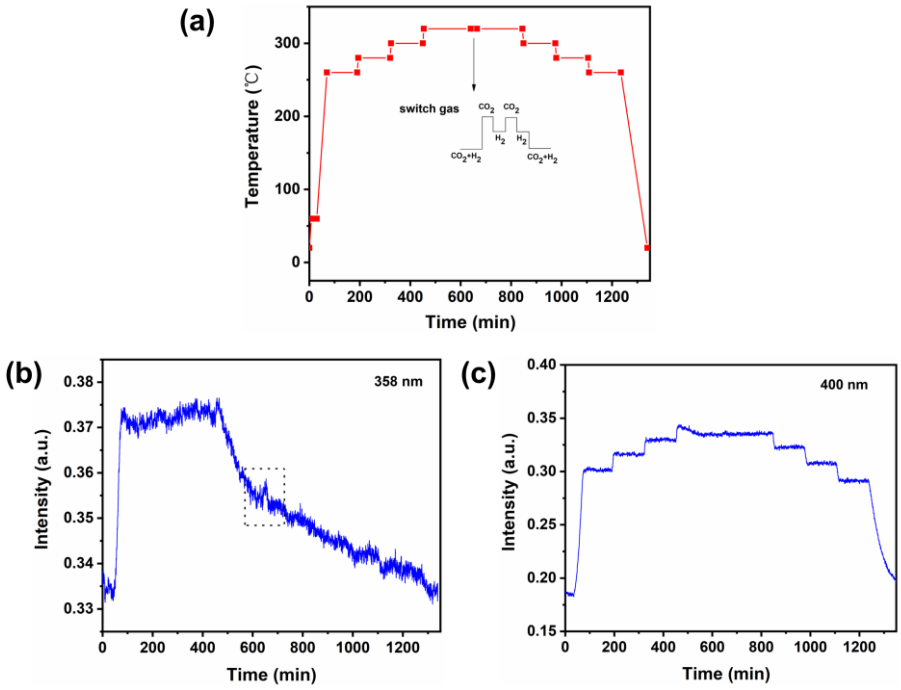

Figure S20. (a) Reaction program of operando UV-Vis DRS measurements under CO_2 hydrogenation reaction conditions. Intensity of the absorption band at ~ 358 nm and (b) ~ 400 nm as a function of reaction time obtained from the operando UV-Vis DRS data of (b) ZnO/ZrO_2-t and (c) ZnO/ZrO_2-m under CO_2 hydrogenation conditions (reaction conditions: 1 bar and gas composition: CO_2/H_2=1/3. grey box: switch gas experiment).

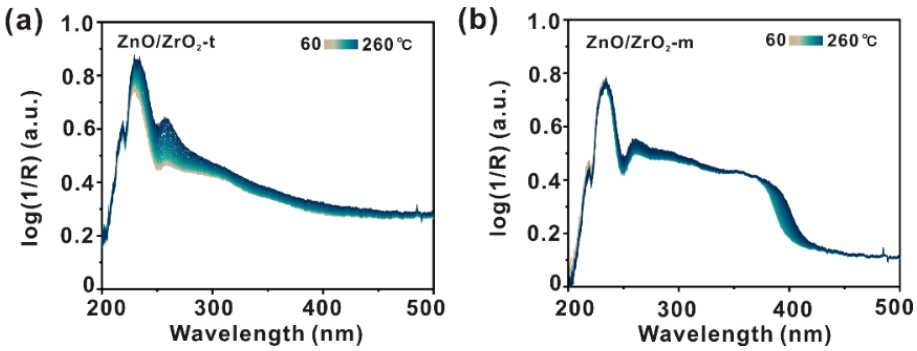

Figure S21. Operando UV-Vis DRS data in the 200-500 nm spectral region obtained for (a) ZnO/ZrO_2-t and (b) ZnO/ZrO_2-m under CO_2 hydrogenation reaction conditions from 60 °C to 260 °C.

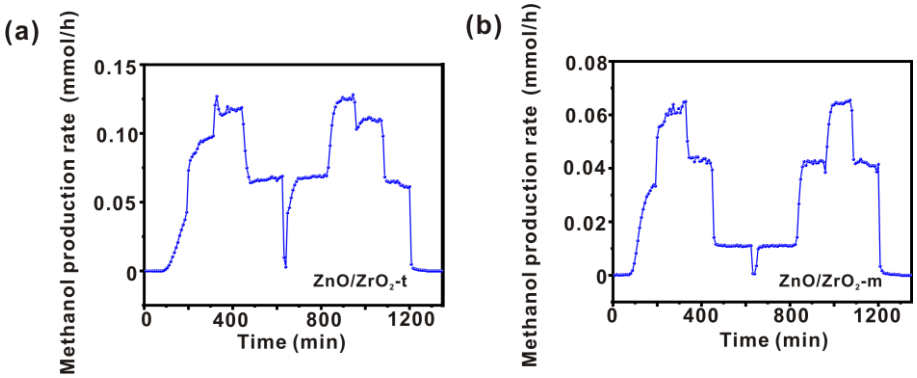

Figure S22. (a) The methanol production rates for ZnO/ZrO_2-t and (b) ZnO/ZrO_2-m (reaction conditions: atmospheric pressure, and gas composition: CO_2/H_2=1/3).

Table S1. Activity comparison of some typical catalyst materials reported in literature under similar conditions. The entries in bold are from this study.

Catalyst	H_2:CO_2 ratio	Temperature (°C)	Pressure (bar)	Methanol selectivity (%)	Space-time yield (mmol g^{-1} h^{-1})
ZnO/ZrO_2-t	**3:1**	**320**	**20**	**81**	**1.25**
ZnO/ZrO_2-m	**3:1**	**320**	**20**	**39**	**0.67**
ZnO/a-ZrO_2[6]	3:1	320	20	43.7	1.16
1In_2O_3-99ZrO_2[7]	4:1	280	50	77	1.87
MOF-808-Zn-4[8]	3:1	250	40	>99	0.95
ZnZrO[9]	3:1	330	20	50	1.44
ZnZrO[10]	3:1	320	40	60	1.56

ZnZr[11]	3:1	290	45	80.5	1.83
$ZnZrO_x$[12]	3:1	325	10	30	0.93
$ZnZrO_x$[13]	3:1	300	10	71	1.90
ZnO_x/ZrO_2[14]	3:1	320	20	67.5	4.68
$5ZnZrO_x$[15]	4:1	320	40	61	4.11
$Cu/m\text{-}ZrO_2$[16]	3:1	250	30	50	0.31
Commercial $Cu/ZnO/Al_2O_3$[17]	3:1	250	30	47.5	17.4
Pd-Cu(0.25)[18]	3:1	250	30	17.5	0.40

5. References

[1] S. Grimme, *J. Comput. Chem.* **2006***, 27*, 1787-1799.

[2] A. Antony, A. Asthagiri, J. F. Weaver, *J. Chem. Phys.* **2013**,*139*, 104702.

[3] C. Ricca, A. Ringuedé, M. Cassir, C. Adamo, F. Labat, *J. Comput. Chem.* **2015**, *36*, 9-21.

[4] R. S. Koster, C. M. Fang, M. Dijkstra, A. van Blaaderen, M. A. Huis, *J. Phys. Chem. C* **2015**, *119*, 5648-5656.

[5] M. Methfessel, A. Paxton, *Phys. Rev. B,* **1989***, 40*, 3616.

[6] L. Lin, G. Wang, F. Zhao, *ChemistrySelect* **2021**, *6*, 2119-2125.

[7] M. S. Frei, C. Mondelli, A. Cesarini, F. Krumeich, R. Hauert, J. A. Stewart, D. Curulla Ferré, J. Pérez-Ramírez, *ACS Catal.* **2019**, *10*, 1133-1145.

[8] J. Zhang, B. An, Z. Li, Y. Cao, Y. Dai, W. Wang, L. Zeng, W. Lin, C. Wang, *J. Am. Chem. Soc.* **2021**, *143*, 8829-8837.

[9] Z. Li, J. Wang, Y. Qu, H. Liu, C. Tang, S. Miao, Z. Feng, H. An, C. Li, *ACS Catal.* **2017**, *7*, 8544-8548.

[10] Z. Li, Y. Qu, J. Wang, H. Liu, M. Li, S. Miao, C. Li, *Joule* **2019**, *3*, 570-583.

[11] D. Xu, X. Hong, G. Liu, *J. Catal.* **2021**, *393*, 207-214.

[12] S. Tada, H. Kinoshita, D. Li, M. Nishijima, H. Yamaguchi, R. Kikcuhi, N. Yamauchi, Y. Kobayashi, K. Iyoki, *Adv. Powder Technol.* **2023***, 34*, 104174.

[13] S. Tada, N. Ochiai, H. Kinoshita, M. Yoshida, N. Shimada, T. Joutsuka, M. Nishijima, T. Honma, N. Yamauchi, Y. Kobayashi, K. Iyoki, *ACS Catal*. **2022**, *12*, 7748.

[14] C. Temvuttirojn, Y. Poo-arporn, N. Chanlek, C.K. Cheng, C.C. Chong, J. Limtrakul, T. Witoon, *Ind. Eng. Chem. Res*. **2020**, *59*, 5525.

[15] T. Pinheiro Araújo, J. Morales-Vidal, T. Zou, M. Agrachev, S. Verstraeten, P.O. Willi, R.N. Grass, G. Jeschke, S. Mitchell, N. López, J. Pérez-Ramírez, *Adv. Energy Mater.* **2023***, 13*, 2204122.

[16] T. Witoon, J. Chalorngtham, P. Dumrongbunditkul, M. Chareonpanich, J. Limtrakul, *Chem. Eng. J*. **2016**, *293*, 327-336.

[17] H. Zhang, J. Chen, X. Han, Y. Pan, Z. Hao, S. Tang, X. Zi, Z. Zhang, P. Gao, M. Li, J. Lv, X. Ma, *Ind. Eng. Chem. Res*. **2024**, *63*, 6210–6221.

[18] X. Nie, X. Jiang, H. Wang, W. Luo, M.J. Janik, Y. Chen, X. Guo, C. Song, *ACS Catal.* **2018**, *8*, 4873–4892.